Langmuir

Article

pubs.acs.org/Langmuir

Coalescence of Two Drops on Partially Wettable Substrates

Min Wook Lee,[†] Dong Kyun Kang,[†] Sam S. Yoon,*[,†] and Alexander L. Yarin*[,‡,§]

[†]Department of Mechanical Engineering, Korea University, Seoul 136-713, Korea

[‡]University of Illinois at Chicago, Department of Mechanical and Industrial Engineering, Chicago, Illinois 60607-7022, United States

[§]Center of Smart Interfaces, Technische Universität Darmstadt, 64287 Darmstadt, Germany

ABSTRACT: The present work contains the results of the experiments with two tiny drops on partially wettable substrates with contact angles of 10°, 24°, 27°, and 56°, which coalesce in the regime entirely dominated by viscous forces. Both side and bottom views are examined. The results for these three-dimensional coalescence flows are compared with scaling laws and the numerical two-dimensional model developed in the present work.

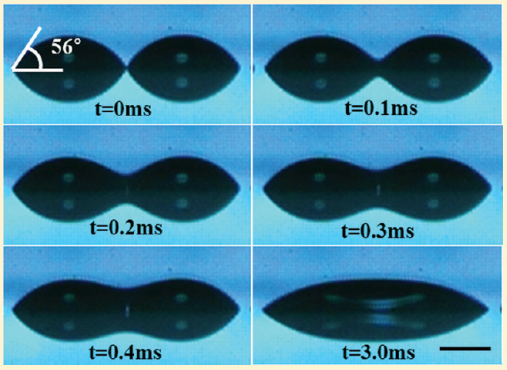

1. INTRODUCTION

Two liquid drops merge together to form a bigger drop or puddle with smaller surface area. This "sintering" of two drops is associated with minimization of the surface energy. This phenomenon is known as *coalescence* or *sintering*, which has many practical applications in low energy fusion of atomic nuclei, molecular clustering, raindrop formation in clouds,[1,2] inkjet printing, drop impact, sprays,[3,4] powder metallurgy,[5] microfluidic devices,[6] and filtration.[7] In the case of spray painting or coating, the coalescence rate of neighboring drops plays a vital role in determining the material properties of the solidified precursor, and therefore, the coalescence is a subject of great interest from the perspective of material science.

Studies of sintering of two free (not touching any solid surface) highly viscous drops date back to the seminal work of Frenkel.[5] When two free drops of any liquid touch each other at their circumference, the flow is initially in the viscous regime because the bridge radius r_m is significantly smaller than the viscous characteristic length, $r_m \ll l_v$, where $l_v = \mu^2/(\gamma\rho)$ with μ, γ, and ρ being liquid viscosity, surface tension, and density. This evolution of the initially singular merging drop profile is ephemeral and, thus, is nearly impossible to observe experimentally or calculate numerically. Once merged, the subsequent evolution of two free drops of low viscosity liquids can rapidly transit to the inertial regime because the neck or bridge radius grows (i.e., $r_m \gg l_v$). In the inertial regime, the merging of two free drops is dominated by the competition between inertia and surface tension, and thus, an inviscid assumption is valid.[4,8,9] The inviscid model shows the bridge between two free drops increases as $r_m \sim t^{1/2}$.

On the other hand, when viscosity is dominant, it slows the coalescence of two free drops, which results in a much longer time scale. In that case, the bridge semiwidth between two free merging cylinders increases, following the law[10−14]

$$\frac{t}{\tau} = \frac{\pi(r_m/R_o)}{4\ln 2 - \ln(r_m/R_o)} \quad (1)$$

which is valid in the range $0 \le (r_m/R_o) \le 0.65$, with R_o being the drop radius and $\tau = \mu R_o/\gamma$.

Significant progress was achieved in the direct numerical simulation of coalescence and sintering in the viscosity-dominated cases using the integral representation of the creeping flow Stokes equations, and a number of important plane and axisymmetric two-dimensional problems were solved by van de Vorst.[13,14] In particular, it was shown that eq 1 for two free cylinders equally well describes coalescence of two free spheres.[14] The same approach can be, in principle, applied to a fully three-dimensional situation; albeit, it is prohibitively time-consuming (cf., for example ref 15).[15]

Coalescence of the two free drops discussed above can differ radically from coalescence of two sessile drops on a substrate, with the latter situation being characteristic of the inkjet application. When the drops wet the substrate, i.e. the contact angle is small, the coalescence dynamics will be significantly affected by viscous stresses imposed by the substrate during the whole process, and significant deviations from the free drop scenario are expected. On partially wettable substrates, the contact angle increases, whereas the coalescence dynamics should tend to that of the free drops.[2,6,16] Several works were devoted to coalescence of two drops on a substrate. In particular, ref 17 dealt with the case of a fully wettable substrate with the contact angle being zero.[17] It was shown that the

Received: August 18, 2011
Published: January 24, 2012

   dx.doi.org/10.1021/la204867c | *Langmuir* 2012, 28, 3791−3798

growth of the semiwidth of the bridge between the two coalescing drops is scaled as $r_m \sim (h_o^{3/2}/R_o)(\gamma t/\mu)^{1/2}$, where h_o and R_o are the maximum height and radius of a fully wetting sessile drop (cf. Figure 1). Reference 17 suggested that the drop

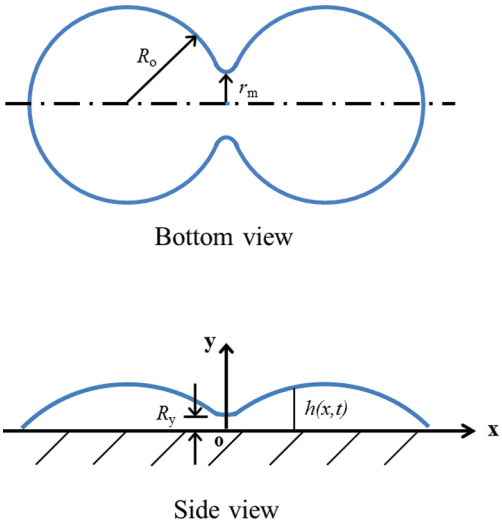

Figure 1. Sketch of coalescence of two drops on a solid surface.

geometry has a vital influence on the coalescence rate. Reference 18 also investigated experimentally and theoretically coalescence of two sessile drops on partially wettable substrates. The scaling law $r_m \sim (\alpha_o R_o^{1/2})(\gamma t/\mu)^{1/2}$ for the bridge semiwidth was suggested. This scaling law was established for the coalescing sessile drops having $25° < \alpha_o < 35°$ contact angle with the partially wettable substrates. It is emphasized that this law cannot be matched with the result of ref 17. Indeed, for small α_o, one expects $\alpha_o = h_o/R_o$, and the scaling law of ref 18 results in $r_m \sim (h_o/R_o^{1/2})(\gamma t/\mu)^{1/2}$ rather than in the above-mentioned result of ref 17. Reference 18 also suggested a model for the height of the bridge, $R_y(t)$, by balancing the viscous stress and the capillary pressure, which yields the bridge growing velocity of $u_b \sim (\gamma/\mu)\alpha_o^2/2$. From this, the bridge height can be estimated as $R_y(t) \sim (\gamma/\mu)\alpha_o^2 t$. It is emphasized that coalescence of two sessile drops represents itself a fully three-dimensional flow.

The present work aims at a further experimental and theoretical investigation of coalescence of two sessile drops on partially wettable substrates. In particular, the evolution of the bridge height $R_y(t)$ is in focus here (cf. Figure 1).

2. EXPERIMENTAL SETUP

Spherical drops in a diameter of the range 100−240 μm [drop volumes in the range $(0.524-7.24) \times 10^{-3}$ cm^3] were generated using the electrohydrodynamic (EHD) inkjet system. Figure 2 is a schematic of the experimental setup for our EHD printing system.

As for a working fluid, diethylene glycol (DEG), was used. The physical parameters of DEG are listed in Table 1, where some additional parameters characterizing the experimental situation are presented (in particular, the expression for the capillary length, $l_\gamma = (\gamma/\rho g)^{1/2}$, g denotes gravity acceleration). For comparison, the corresponding parameters from ref 17 are reproduced. Table 1 shows that in the present experiments much smaller drops are used than those in ref 17. In the present experiments the bridge height $R_y \sim (0.1-0.4)R_o$. Taking for the estimate $R_o = 240$ μm, we obtain $R_y \sim 24-96$ μm. Using the data from Table 1, we find that in the present case the drop size $R_y \ll l_\gamma$, which guarantees a negligibly small gravity effect. In addition, R_y is close to l_ν, which shows that we are still dealing with the viscosity-dominated creeping flow coalescence regime.

The working fluid was supplied to the stainless-steel nozzle (EFD, inner and outer diameters of 0.25 and 0.52 mm, respectively) by a syringe pump (KDS 100). All experiments were performed at room temperature (i.e., $T = 24.2$ °C).

To vary the contact angle of a deposited drop, various substrates were used: platinum (PT)-coated ITO, HMDS-coated ITO, thin-ITO, and thick-ITO substrates which yield the equilibrium static contact angles of $\alpha_o = 10°$, 24°, 27°, and 56°, respectively. Note that the thin- and thick-ITO substrates had the surface roughnesses of 0.52 and 0.70 μm, respectively, based on the AFM images (not shown here); the latter one yielded the larger contact angle of 56°. The contact angles were measured prior to start of the coalescence of the two drops, and they were verified with the measurements of static contact angles of single drops deposited on these substrates. Before drops were deposited, all substrates were washed with ethanol for 3−5 min in an ultrasonic bath and then dried with pure nitrogen gas. The time lapses between the depositions of the first and second adjacent drops were 1 s, 0.35 s, 45 ms, and 3 ms for $\alpha_o = 10°$, 24°, 27°, and 56°, respectively.

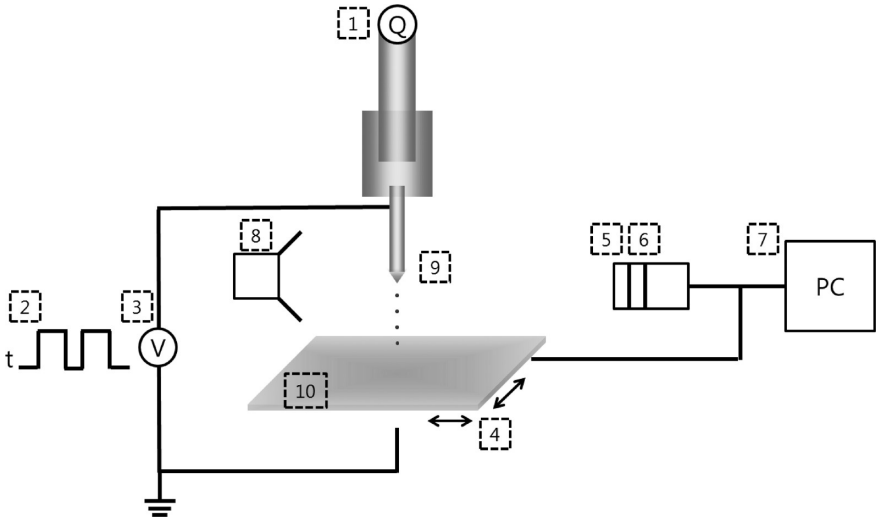

Figure 2. Schematic of the experimental setup: 1, syringe pump; 2, multifunction synthesizer; 3, ac amplifier; 4, X−Y stage; 5, zoom lens; 6, high-speed camera; 7, control PC; 8, light source; 9, nozzle; 10, substrate.

dx.doi.org/10.1021/la204867c | Langmuir 2012, 28, 3791−3798

Table 1. Liquid Properties and the Corresponding Parameters

parameter	fluid	R_o (μm)	ρ (kg/m^3)	μ (mPa·s)	γ (mN/m)	γ/μ (m/s)	$l_\gamma = (\gamma/\rho g)^{1/2}$ (mm)	$l_v = \mu^2/\rho\gamma$ (mm)	$Re_\mu = \rho R_o \gamma/\eta^2$
present work	DEG	110.5−240	1118	38.5	43.16	1.12	1.98	0.03	$3.59 < Re_\mu < 7.82$
ref 17	silicone oil	5000	970	100, 350, 1000	20	0.2, 0.06, 0.02	1.45	0.515, 6.314, 51.55	$0.097 < Re_\mu < 9.7$

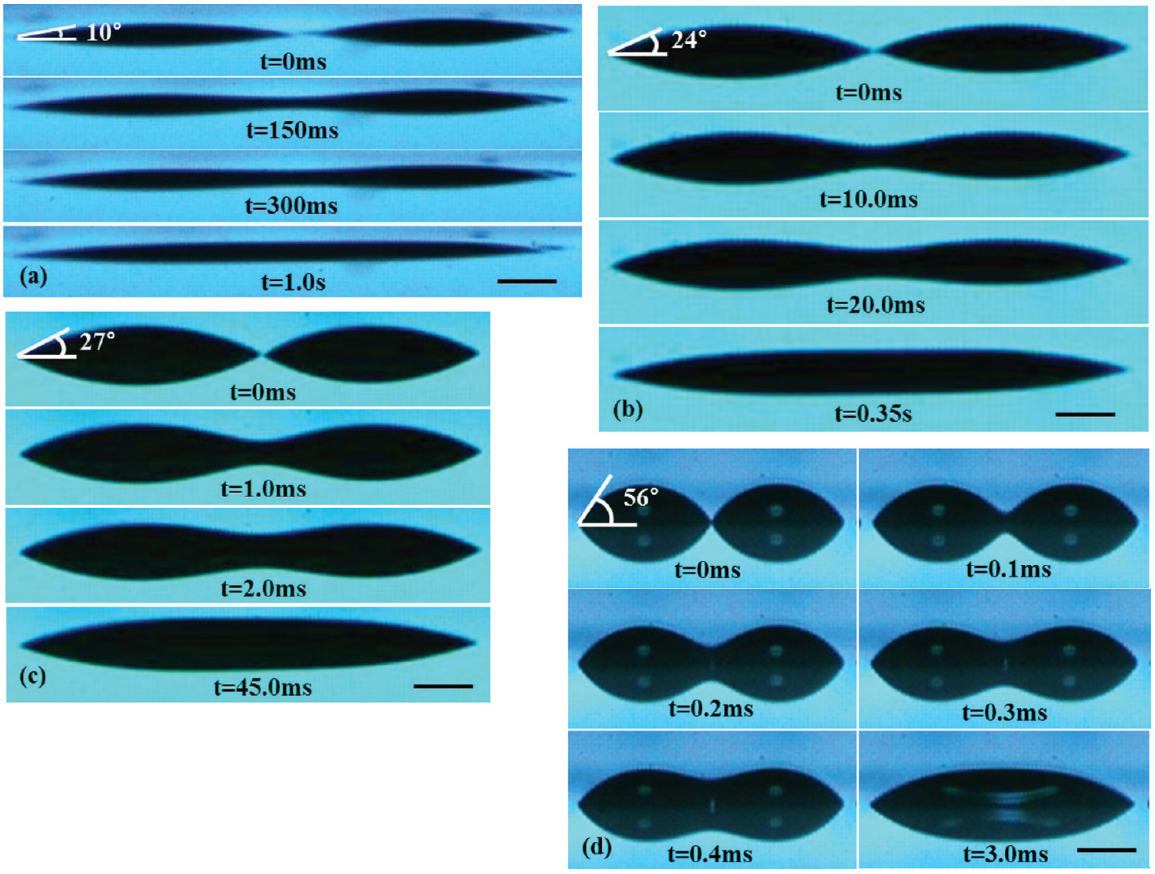

Figure 3. Side-view images of two coalescing DEG sessile drops. The time moments from the beginning of the process are listed in the images; scale bar = 100 μm. The nozzle inner diameter of 0.25 mm was used, which produced the deposited drop size in the range of 110.5 μm < R_o < 240 μm. (a) The static contact angle of 10° on PT-coated ITO substrate with R_o = 240 μm, yielding $\tau = \mu R_o/\gamma$ = 0.2141 ms. (b) The static contact angle of 24° on HMDS-coated glass substrate with R_o = 225 μm, yielding $\tau = \mu R_o/\gamma$ = 0.2007 ms. (c) The static contact angle of 27° on thin-ITO substrate with R_o = 199 μm, yielding $\tau = \mu R_o/\gamma$ = 0.1775 ms. (d) The static contact angle of 56° on thick-ITO substrate with R_o = 110.5 μm, yielding $\tau = \mu R_o/\gamma$ = 0.0986 ms. All the values of the time scale τ are combined in Table 3.

The impact velocities estimated from the images were on the scale of 10 m/s.

The nozzles listed in the caption to Figure 3 were used to record side views of coalescing drops. In the additional experiments when side and bottom views were recorded simultaneously, a bigger nozzle was used because of the requirement of a dual camera setup: one for the side view and the other for the bottom view. Such experiments were done only with *transparent* thick-ITO substrate: Note that the other substrates were nontransparent and bottom view observations were impossible with them. Furthermore, the top views were also impossible because of the nozzle located straight above the coalescing drops. In the case of the thick-ITO substrate with the contact angle of 56°, the nozzle inner diameter and the flow rate were, respectively, 0.25 mm and 10 μL/h, in the case of the side view observations. Then, the deposited drop size was R_o = 110.5 μm. For the simultaneous side and bottom view observations, the nozzle inner diameter and the flow rate were, respectively, 0.33 mm and 50 μL/h. Then, the deposited drop size was R_o = 240 μm. Remarkably, the recorded ratios for the side view R_y/R_o were practically the same for both nozzles, which ascertains the fact that the bigger drops were still pretty close to l_v; that is, coalescence was practically viscosity-dominated.

A multifunction synthesizer (NF Corporation, WF 1973) generated a rectangular step-function signal, which was sent to the HV-amplifier (TREK 10/40A) for thousand-fold amplification. The width of the rectangular signal (duty ratio) was held constant at 2 ms. No baseline (or bias) low-voltage was applied, although this could facilitate preloading of the liquid meniscus for easier drop ejection at each voltage peak.

A high-speed camera (Vision Research, Inc., Phantom 7.3) with a zoom lens (1.56 μm/pixel) and LED lamp (50 W) captured magnified images of ejected DEG drops. In recording the side views, the camera was aligned at the same vertical level as that of the substrate and the distance between the lens and the merging drops was less than 2 cm. The camera image was purposely centered at the merging location to minimize error due to a potential skewed camera angle. The error in measuring the location of points at the drop surface was less than 1°. Snapshots were taken at the interval range 100−220 μs, depending on how the time scale varied with the contact angle. The motorized stage holding the substrate (Future Science, FS-XY-0.1-100) was maneuvered with increments of 0.1-μm. After the first drop was injected, the second drop was injected and placed right next to the first one by maneuvering the motorized stage. The distance

dx.doi.org/10.1021/la204867c | *Langmuir* 2012, 28, 3791−3798

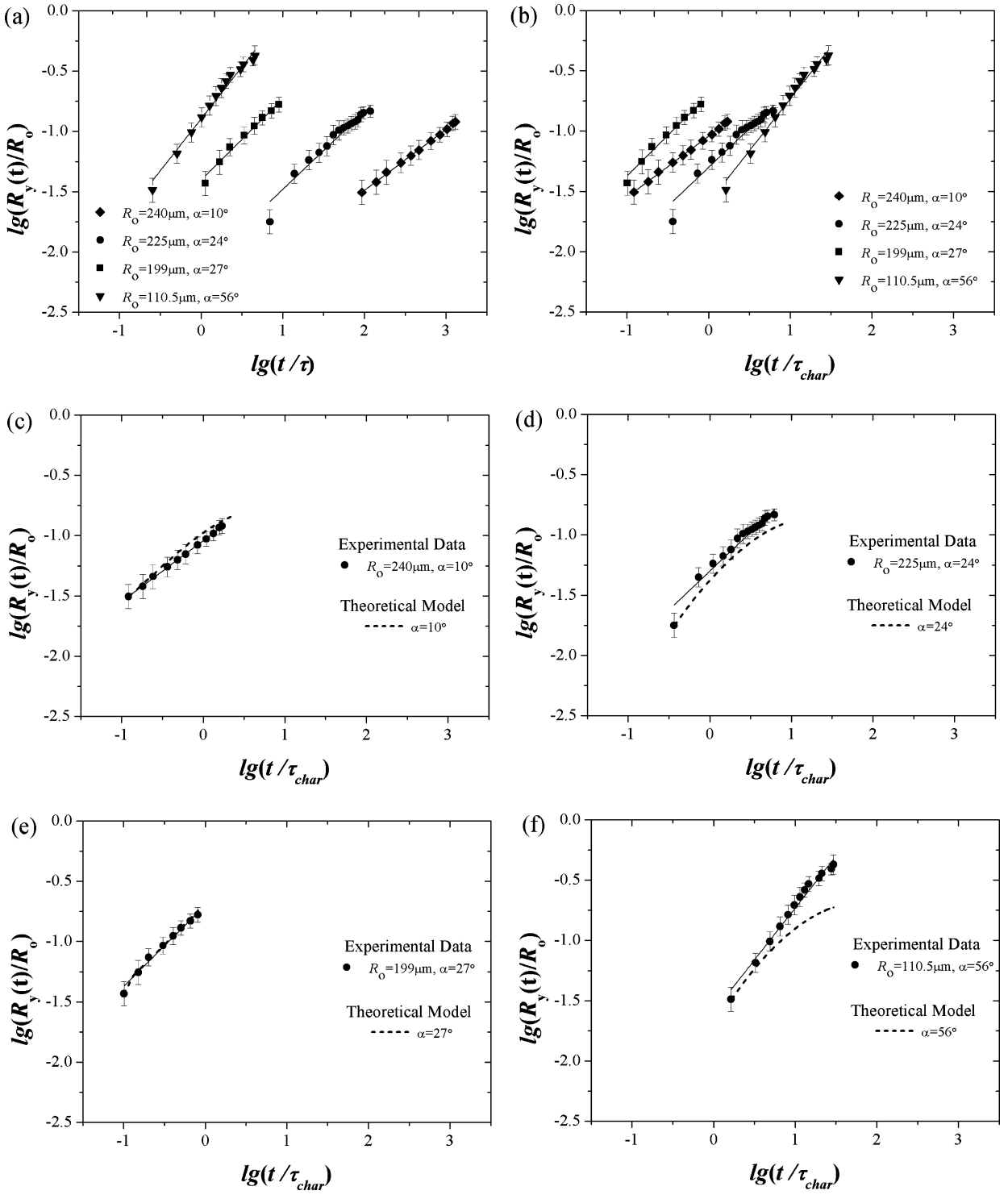

Figure 4. Bridge height versus time. (a) Raw data for the equilibrium static contact angles of 10°, 24°, 27°, and 56° with the time scale $\tau = \mu R_o/\gamma$. The straight lines show the scaling of eq 16 with the values of a and b given in Table 2. (b) Data for the same static contact angles with the time scale $\tau_{char} = \tau/[^4/_3 \tan^4 \alpha_o]$; cf. eq 12. The straight lines show the scaling of eq 17 with the values of c and d given in Table 4. The experimental data are compared with the numerical results in panels c–f, which correspond to 10°, 24°, 27°, and 56°, respectively. The spanning straight lines represent the scaling law (eq 17), with the values of c and d given in Table 4. In panels a–f the data are shown with the symbols and the scaling and numerical results by lines explained in the panels and captions. All the values of the time scales τ and τ_{char} are listed in Table 3. Note that the nozzle used for all of these experiments in Figure 4 has the inner and outer diameters of 0.25 and 0.52 mm, respectively. All of the injected drops retained the same size prior to impact, after which, however, their contact angle difference yielded different sessile drop sizes, R_o, listed in the caption to Figure 3.

between the nozzle tip and the substrate was fixed at H = 2 mm. In all the experiments, time was recorded from the moment of the deposition of the second drop. That moment was assumed to be the initial moment of the coalescence process. It is emphasized that, practically, the initial moment of coalescence is very hard to fully fix, since drops could slightly overlap or, on the contrary, reach each other in the course of a transient spreading over the substrate.

dx.doi.org/10.1021/la204867c | *Langmuir* 2012, 28, 3791–3798

3. THEORETICAL MODEL

3.1. Governing Equations. Shallow sessile drops of viscous fluid in contact with each other coalesce due to the action of surface tension. In the present experiments, drop coalescence is strongly affected not only by viscous bulk stresses but also by viscous friction with the substrate. Thus, the process should deviate significantly from the coalescence of highly viscous free drops. Flows developing in coalescing shallow sessile drops are kindred to those in thin liquid films and are prone to a description in the framework of the lubrication approximation. In general, the coalescence process depicted in Figure 1 is three-dimensional. It is tempting, however, to describe it as a planar flow in the side view, as in the case of the coalescence of two infinitely long and parallel liquid lines, and to discuss possible three-dimensional effects a posteriori.

The lubrication equation for thin viscous films affected by surface tension and viscosity derived in ref 19 for a curved cylindrical surface (a film on a filament) readily reduces to the planar case of interest and takes the following form (cf. ref 17)

$$\frac{\partial h}{\partial t} + \frac{\gamma}{3\mu}\frac{\partial}{\partial x}\left(h^3 \frac{\partial^3 h}{\partial x^3}\right) = 0 \tag{2}$$

where t is time, x is the coordinate reckoned along the substrate, and $h(x,t)$ is the drop profile.

The origin of the x axis is taken at the center between the two drops (cf. Figure 1), which implies the following two boundary conditions

$$x = 0: \quad \frac{\partial h}{\partial x} = 0, \quad \frac{\partial^3 h}{\partial x^3} = 0 \tag{3}$$

It is emphasized that while the first boundary condition (eq 3) expresses the symmetry assumed between two coalescing drops, the second one follows from the mass conservation during the coalescence process, since any solution of eq 2 should possess the integral invariant

$$\int_0^{2R_o} h(x)\,dx = \int_0^{2R_o} h_o(x)\,dx = \text{const} \tag{4}$$

where $x = 2R_o$ stands for the drop width (cf. Figure 1) and the initial drop profile is given by the initial condition

$$t = 0: \quad h = h_o(t) \tag{5}$$

The additional two boundary conditions required for eq 2 are imposed at the contact line as

$$x = 2R_o: \quad h = 0, \quad \frac{\partial h}{\partial x} = -\tan \alpha_o \tag{6}$$

where α_o is the static contact angle.

Practically it is convenient to describe the initial drop profile by two tangent parabolas—concave in the bridge and convex in most of the drop. Therefore, rendering h_0, x, R_y, and x_m dimensionless by R_o, we take at $0 \le x \le x_m$:

$$h_o(x) = R_y + Cx^2 + Dx; \text{ with}$$

$$C = \frac{R_y - (1/2)x_m^2 \tan \alpha_o}{x_m^2} > 0,$$

$$D = -2Cx_m - x_m \tan \alpha_o + \tan \alpha_o \tag{7}$$

and at $x_m < x \le 2$:

$$h_o(x) = -(1/2)x^2 \tan \alpha_o + x \tan \alpha_o \tag{8}$$

In eqs 7 and 8 R_y is the dimensionless bridge height and x_m is sufficiently smaller than 2, i.e. $x_m = 0.1$. It is emphasized that the initial drop shapes in the form of eqs 7 and 8 rapidly readjust themselves to the shapes admitted by eq 2. These readjusted drop shapes lead to monotonous growth in bridge height and thus form self-consistent initial conditions.

The last condition (eq 6) implies that flow developing predominantly in the bridge between two coalescing drops practically does not affect the domain near the contact line where fluid is at rest and the static contact angle is preserved.

3.2. Local Analysis of the Initial Evolution of the Bridge. Consider the initial flow development in the established bridge between two coalescing drops. In this case locally (in the bridge) eq 2 can be linearized and reduced to the following dimensionless form

$$\frac{\partial h}{\partial t} + \varepsilon^3 \frac{\partial^4 h}{\partial x^4} = 0 \tag{9}$$

where x and h are rendered dimensionless by R_o and t by $3\mu R_o/\gamma$. In addition, $\varepsilon = R_{y0}/R_o \ll 1$ is the small parameter based on the initial bridge height R_{y0}.

Stretching the spatial coordinate,[20] we find the inner solution of eq 9 in the bridge

$$h = \varepsilon \exp\left(\omega t + \frac{\omega^{1/4}}{\sqrt{2}}\frac{x}{\varepsilon}\right)\cos\left(\frac{\omega^{1/4}}{\sqrt{2}}\frac{x}{\varepsilon}\right) \tag{10}$$

which can be matched with the outer shape of the drop at this initial stage of coalescence (eq 8).

The matching allows finding ω as

$$\omega = 4 \tan^4 \alpha_o \tag{11}$$

Equation 11 shows that the characteristic time of the initial evolution of the established bridge is

$$\tau_{char} = \frac{\mu R_o}{\gamma}\frac{1}{(4/3)\tan^4 \alpha_o} \tag{12}$$

3.3. Bridge Width. The two-dimensional coalescence outlined above can be valid only if the outflow to the third dimension from the bridge region is relatively weak. To evaluate the rate of such lateral flow, use should be made of the Hoffman–Tanner–Voinov law for partially wettable surfaces[21,22]

$$\alpha^3 - \alpha_o^3 = 72.67\text{Ca} \tag{13}$$

where α is the dynamic contact angle and the capillary number $Ca = \mu U/\gamma$, with U being the velocity of the bridge contact line in the lateral direction.

dx.doi.org/10.1021/la204867c | Langmuir 2012, 28, 3791−3798

According to eq 13, the rate of the bridge widening is found from the following equation

$$\frac{dr_m}{dt} = U \approx \frac{\gamma}{\mu} 0.0138 \left(\frac{R_{y0}}{r_m}\right)^3 \quad (14)$$

where $\alpha \approx (R_y/r_m) \gg \alpha_o$.

The integration of eq 14 results in the following scaling law

$$r_m = 0.485 \left(\frac{\gamma R_{y0}^3}{\mu}\right)^{1/4} t^{1/4} \quad (15)$$

4. RESULTS AND DISCUSSION

An example of a succession of side-view images of two small merging drops recorded in the experiments is presented in Figure 3. Such images were treated as two-dimensional (neglecting the effect of the camera tilt, which introduced an error of about 1%) and used to acquire data on the surface elevation during the coalescence process $h(x,t)$. In particular, the experimental results for the middle of the bridge height $R_y(t) = h(0,t)$ are presented in Figure 4a–f. The data in Figure 4a roughly reveal the scaling behavior as

$$R_y/R_o = a(t/\tau)^b \quad (16)$$

where the values of a and b are presented in Table 2; albeit, for the contact angles of 24°, 27°, and 56° this simple scaling is

Table 2. Scaling Factors in Eq 16

contact angle	a	b
10°	0.0032	0.5061
24°	0.0067	0.6435
27°	0.0396	0.6719
56°	0.1254	0.8612

incapable of approximating the entire duration of the experiment. It shows that, for the lowest contact angle of 10°, the scaling for the bridge height is similar to the one found in ref 17 ($\sim t^{1/2}$, albeit for the bridge width r_m, rather than the height R_y) in the fully wettable case. However, as the contact angle increases, the scaling for the bridge height demonstrates the exponent values in the range $0.51 < b < 0.86$ (note that ref 18 produced the scaling $R_y \sim t$). It is emphasized that eq 1 for coalescing free drops being used with R_y instead of r_m does not describe the data in Figure 4. This shows that the dynamics of the coalescence process revealed in Figure 4 is significantly affected by the presence of the substrate and the associated viscous stresses.

The inspection of the time values listed in Figure 3 reveals that the time scale $\tau = \mu R_o/\gamma$ listed in Table 3 can hardly be

Table 3. Time Scales $\tau = \mu R_o/\gamma$ and $\tau_{char} = \tau/[^4/_3 \tan^4 \alpha_o]$ of Eq 12

contact angle	τ, ms	τ_{char}, ms	τ_{char}/τ
10°	0.214	166.04	775.9
24°	0.201	3.831	19.1
27°	0.178	1.975	11.1
56°	0.099	0.015	0.15

considered as the characteristic time of the coalescence process. On the other hand, the values of the time scale $\tau_{char} = \tau/[^4/_3 \tan^4 \alpha_o]$, which is the characteristic time scale of the initial evolution of the bridge according to eq 12, are listed in Table 3. The rescaling of the experimental data versus t/τ_{char} rather than versus t/τ groups the data much more compactly (cf. Figure 4a and b). This implies that most of the coalescence process corresponds to the initial evolution of the bridge described in subsection 3.2 rather than to the fast ultimate merging of two drops recorded in Figure 3. As was explained in section 2, the initial moment of the coalescence process is practically impossible to measure due to the small spatial inaccuracies of the deposition of the second drop. On the other hand, the temporal inaccuracies brought by these small spatial inaccuracies can still be significant (on the scale of one order of magnitude, as Figure 4b reveals), since the initial bridge evolution is the longest stage of the coalescence process.

Table 4. Scaling Factor in Eq 17: Experimental Data

contact angle	c	d
10°	0.0911	0.5061
24°	0.0481	0.6435
27°	0.1988	0.6719
56°	0.0262	0.8612

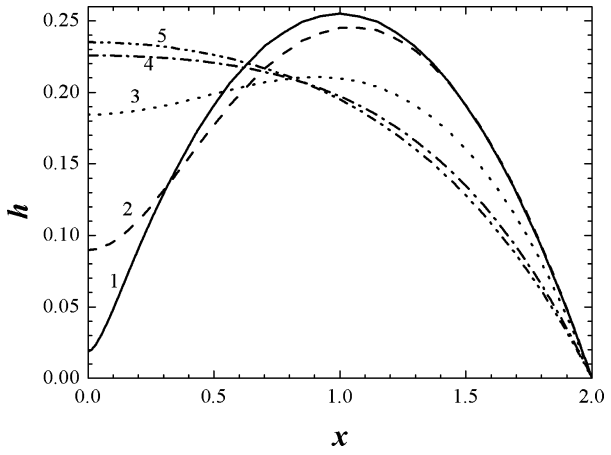

Figure 5. Drop shapes during the coalescence process in the case of the contact angle of 27°. Curves 1–5 correspond to t/τ_{char} = 0.03, 0.49, 1.99, 3.99, and 4.99, respectively (which are equivalent to t = 0.0395, 0.968, 3.93, 7.88, and 9.855 ms in dimensional time); cf. Figure 3c.

To describe the entire coalescence process, eq 2 was discretized in the x-direction and the resulting system of the ordinary differential equations for the profile values $h_i(t)$ corresponding to the nodes x_i was solved numerically using the Kutta–Merson method. The corresponding numerical solution of the problem (eqs 2–8) revealed the results shown in Figure 4c–f. The experimental results shown in Figure 4b–f can be presented as the scaling law

$$R_y/R_o = c(t/\tau_{char})^d \quad (17)$$

with the parameters c and d listed in Table 4.

It is emphasized that the values of the drops radius R_o available from the experiments can be considered only as an estimate from the point of view of the two-dimensional numerical model. Therefore, a total superimposition of the experimental and numerical data in Figure 4c–f should not be expected. To compare the predicted numerical trends with the

dx.doi.org/10.1021/la204867c | Langmuir 2012, 28, 3791–3798

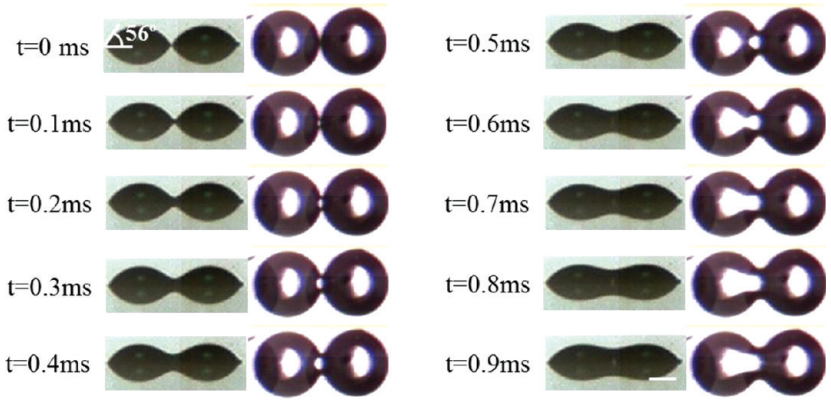

Figure 6. Simultaneously recorded side- and bottom-view images of two coalescing sessile drops. DEG on thick ITO substrate. The time interval is 0.1 ms, static contact angle of 56°. R_o = 240 μm, $\tau = \mu R_o/\gamma$ = 0.2141 ms, scale bar = 200 μm.

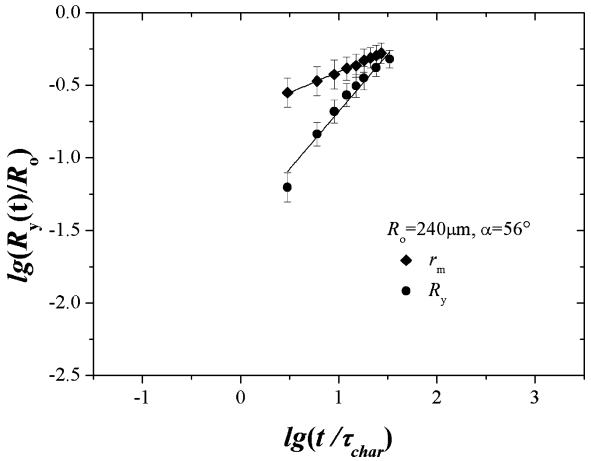

Figure 7. Simultaneously measured bridge width r_m and height R_y versus time for the contact angle of α_0 = 56°. The experimental data are shown by symbols. The scaling laws are shown by the corresponding straight lines. Note that the nozzle used for all these experiments had the inner and outer diameters of 0.33 and 0.65 mm, respectively, which produced a sessile drop size of R_o = 240 μm because of the larger nozzle diameter (0.33 mm) and larger flow rate (50 μL/h) in comparison with the conditions used in Figure 4 (0.25 mm and 10 μL/h, respectively).

experimental data, the numerical curves were shifted vertically in Figure 4c–f to the first experimental point on the left. It is seen that the general shape of the experimental and numerical dependences depicted in Figure 4c–f reveals a fairly good agreement; albeit, for the contact angle of 56° a growing deviation is observed in Figure 4f. This deviation probably results from the fact that for drops with such large contact angle the lubrication approximation of eq 2 becomes less accurate.

Several numerically predicted shapes of one of the two coalescing drops are shown in Figure 5. The results are in fairly good agreement with the data in Figure 3c.

The side- and bottom-view images recorded simultaneously for the case of the contact angle of 56° are presented in Figure 6. The corresponding time dependences for the bridge width r_m and height R_y are shown in Figure 7. The data are traced by the corresponding scaling laws. In particular, eq 17 represents the data for R_y/R_o with c = 0.0345 and d = 0.7892. The value of the exponent d agrees fairly well with the corresponding value for the contact angle of 56° in Table 4 (d = 0.8612). On the other hand, the data for r_m/R_o in Figure 7 corresponds to the following scaling law

$$r_m/R_o = e(t/\tau_{char})^f \quad (18)$$

with e = 0.2006 and f = 0.2901. It is emphasized that this experimental scaling remarkably agrees with the prediction of eq 15, and the dependence of r_m on t corresponding to the theoretical eq 15 ($r_m \sim t^{1/4}$) or the experimental data of eq 18 ($r_m \sim t^{0.29}$) is significantly weaker than the one of ref 18 ($r_m \sim t^{1/2}$) for partially wettable substrates.

The results in Figure 7 show that the bridge height begins to increase on the background of a very slowly widening bridge, which validates the two-dimensional model outlined in section 3 to describe the evolution of the bridge height.

5. CONCLUSION

The experiments with the side-view recording of two coalescing drops on partially wettable substrates with the contact angles of 10°, 24°, 27°, and 56° showed that the increase of the bridge height in time can be roughly represented with the power law $R_y/R_o = c(t/\tau_{char})^d$ with the characteristic time $\tau_{char} = (\mu R_o/\gamma)/[^4/_3 \tan^4 \alpha_o]$ and the exponent d from the range $0.5061 \le d \le 0.8612$. It is emphasized that only at 10° does the entire data set follow the scaling law, whereas at 24°, 27°, and 56° the data ultimately deviate from this law at longer times. The present experiments were conducted with drops sufficiently small that the entire coalescence process corresponds to the viscosity-dominated creeping flow regime. The known result for coalescence of two free drops, eq 1, does not describe the data for coalescence of two sessile drops on partially wettable substrates. The latter ascertains the important role of the viscous shear stresses associated with the substrate.

The experiments with the simultaneous side- and bottom-view recording of two coalescing drops with the contact angle of 56° revealed the following scaling law for the bridge width: $r_m/R_o = e(t/\tau_{char})^f$, with e = 0.2006 and f = 0.2901. It is shown that this law follows from the Hoffman–Tanner–Voinov law for partially wettable surfaces. The bridge width forms much faster than the bridge height evolves, which validates the two-dimensional planar model introduced for the bridge height prediction.

The two-dimensional description of the entire coalescence process of two drops in the framework of the lubrication approximation revealed the trends for the bridge height, which

dx.doi.org/10.1021/la204867c | Langmuir 2012, 28, 3791–3798

are in fairly good agreement with the experimental data for different contact angles.

AUTHOR INFORMATION

Corresponding Author

*E-mail: skyoon@korea.ac.kr; E-mail: ayarin@uic.edu.

ACKNOWLEDGMENTS

This work was supported by the Center for Inorganic Photovoltaic Materials (NRF-2011-0007182 and 2010-0010217), funded by the Korean government (MEST). This research was also supported by the Converging Research Center Program through the Ministry of Education Science and Technology (2010K000969) and by the Research Center of Breakthrough Technology Program through the Korea Institute of Energy Technology Evaluation and Planning (KETEP), funded by the Ministry of Knowledge Economy (2009-3021010030-11-1).

REFERENCES

(1) Bradley, S. G.; Stow, C. D. Collisions between liquid drops. *Philos. Trans. R. Soc. London, Ser. A: Math., Phys. Sci.* **1978**, *287* (1349), 635−675.

(2) Menchaca-Rocha, A.; Martinez-Davalos, A.; Nunez, R. Coalescence of liquid drops by surface tension. *Phys. Rev. E* **2001**, *63*, 046309.

(3) *Handbook of Atomization and Sprays*; Ashgriz, N., Ed.; Springer: Heidelberg, NY, 2011.

(4) Duchemin, L.; Eggers, J.; Josserand, D. C. Inviscid coalescence of drops. *J. Fluid Mech.* **2003**, *487*, 167−178.

(5) Frenkel, J. Viscous flow of crystalline bodies under the action of surface tension. *J. Phys. (Moscow)* **1945**, *9*, 385−391.

(6) Wu, M.; Cubaud, T.; Ho, C. M. Scaling law in liquid drop coalescence driven by surface tension. *Phys. Fluids* **2004**, *16* (7), L51−L54.

(7) Yarin, A. L.; Chase, G. G.; Liu, W.; Doiphode, S. V.; Reneker, D. H. Liquid drop growth on a fiber. *AIChE J.* **2006**, *52*, 217−227.

(8) Eggers, J. Coalescence of spheres by surface diffusion. *Phys. Rev. Lett.* **1998**, *80* (12), 2634−2637.

(9) Eggers, J.; Lister, J. R.; Stone, H. A. Coalescence of liquid drops. *J. Fluid Mech.* **1999**, *401*, 293−310.

(10) Hopper, R. W. Plane Stokes flow driven by capillarity on a free surface. *J. Fluid Mech.* **1990**, *213*, 349−375.

(11) Hopper, R. W. Plane Stokes flow driven by capillarity on a free surface. Part 2. Further developments. *J. Fluid Mech.* **1991**, *230*, 355−364.

(12) Hopper, R. W. Coalescence of two viscous cylinders by capillarity: Part I, Theory. *J. Am. Ceram. Soc.* **1993**, *76* (12), 2947−2952.

(13) van de Vorst, G. A. L. Integral method for a two-dimensional Stokes flow with shrinking holes applied to viscous sintering. *J. Fluid Mech.* **1993**, *257*, 667−689.

(14) van de Vorst, G. A. L. Modeling and Numerical Simulation of Viscous Sintering. TU Eidhoven, 1994.

(15) Reznik, S. N.; Salalha, W.; Yarin, A. L.; Zussman, E. Microscale fibre alignment by a three-dimensional sessile drop on a wettable pad. *J. Fluid Mech.* **2007**, *574*, 179−207.

(16) Thoroddsen, S. T.; Takehara, K.; Etoh, T. G. The coalescence speed of a pendent and a sessile drop. *J. Fluid Mech.* **2005**, *527*, 85−114.

(17) Ristenpart, W. D.; McCalla, P. D.; Roy, R. V.; Stone, H. A. Coalescence of spreading drops on a wettable substrate. *Phys. Rev. Lett.* **2006**, *97*, 064501.

(18) Narhe, R. D.; Beysens, D. A.; Pomeau, Y. Dynamic drying in the early-stage coalescence of drops sitting on a plate. *Europhys. Lett.* **2008**, *81*, 46002.

(19) Yarin, A. L.; Oron, A.; Rosenau, P. Capillary instability of thin liquid film on a cylinder. *Phys. Fluids A* **1993**, *5* (1), 91−98.

(20) van Dyke, M. *Perturbation Methods in Fluid Mechanics*; Academic Press: New York, 1964.

(21) Tanner, L. H. The spreading of silicone oil drops on horizontal surfaces. *J. Phys. D: Appl. Phys.* **1979**, *12*, 1473−1484.

(22) Kistler, S. F. Hydrodynamics of wetting. In *Wettability*; Marcel Dekker: New York, 1993; pp 311−429.